Lawrence Berkeley Laboratory
UNIVERSITY OF CALIFORNIA

Materials & Molecular
Research Division

Submitted to the Journal of Chemical Physics

CHEMILUMINESCENT CHEMI-IONIZATION: Ar* + Ca AND THE $CaAr^+$ EMISSION SPECTRUM

Dennis C. Hartman and John S. Winn

September 1980

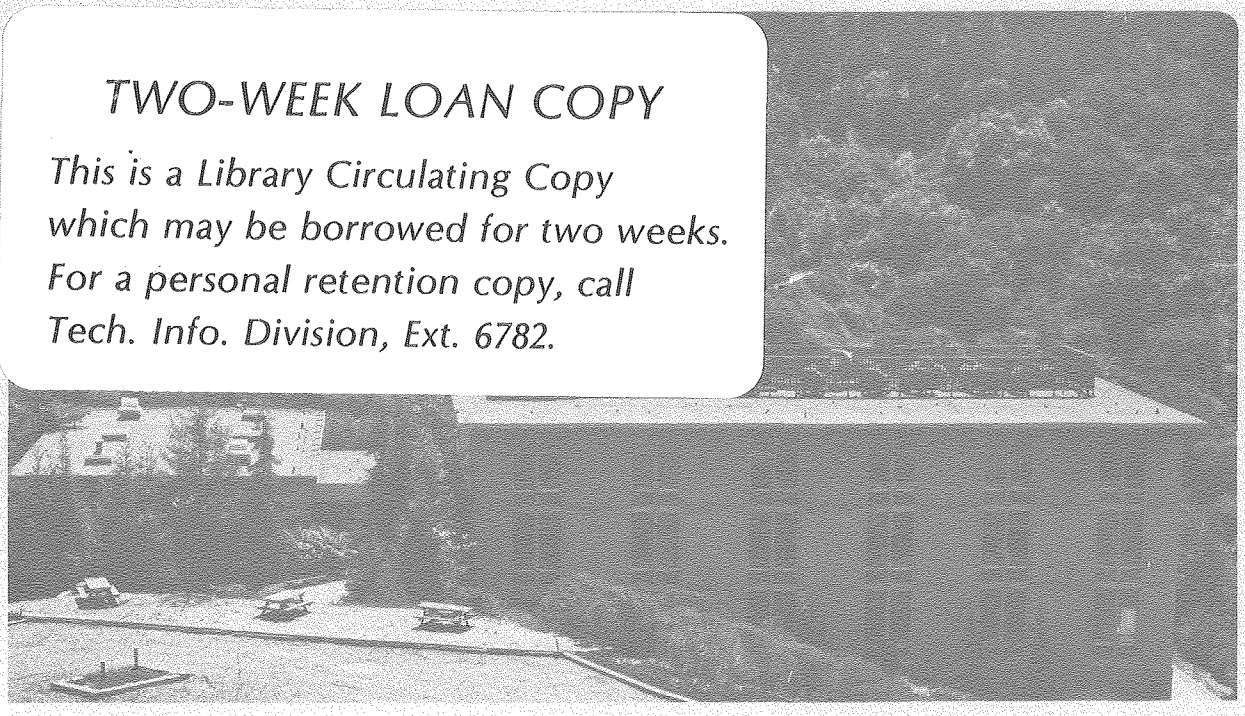

Prepared for the U.S. Department of Energy under Contract W-7405-ENG-48

DISCLAIMER

CHEMILUMINESCENT CHEMI-IONIZATION: $Ar^* + Ca$ and the $CaAr^+$ Emission Spectrum

by

Dennis C. Hartman[a] and John S. Winn[b]

Department of Chemistry and
Materials and Molecular Research Division
Lawrence Berkeley Laboratory
University of California, Berkeley, CA 94720

a) Present address: Central Research Laboratories, Texas Instruments, Inc., Dallas, Texas 75265

b) Alfred P. Sloan Research Fellow

Abstract

A flowing afterglow chemilumunescence apparatus has been used to analyse visible fluorescence in the Ar* ($^3P_2^o$) + Ca ($^1S_0$) reaction. The rate constants for production of Ca^+ ($^2P_{3/2}^o$) and Ca^+ ($^2P_{1/2}^o$) were measured to be 1.6×10^{-10} cm^3-$molecule^{-1}$ sec^{-1} and 3.2×10^{-11} cm^3 $molecule^{-1}$ sec^{-1}, respectively. These results demonstrate a transfer of the total electronic angular momentum polarization in Ar* to the excited ion levels. The molecular band spectrum of the associative ionization product $CaAr^+$ ($A^2\Pi$) was observed. Molecular fluorescence constituted 14% of the total fluorescence from all ion products. This spectrum was analyzed with a model (exp-Z4) potential, yielding, for the ground state, $X^2\Sigma^+$, $R_e = 2.8$ Å, $\omega_e'' = 87$ cm^{-1}, and $D_e'' = 1000$ cm^{-1}, and, for the $A^2\Pi$ state, $R_e = 2.6$ Å, $\omega_e' = 200$ cm^{-1}, and $D_e' = 4900$ cm^{-1}. The nascent internal state distribution in $CaAr^+$ is found to consist of a fairly narrow range of high vibrational levels.

The analysis of spectra from chemiluminescent reaction is a well established technique for elucidating the product state distributions of elementary processes. In this paper, we use the analysis of the chemiluminescent chemi-ionization reactions between metastable argon atoms and calcium atoms to expose the dynamics of associative ionization (AI) and to measure the branching ratios for chemi-ionization into more than one product channel.

The system we have chosen, Ar^* (^3P) + Ca (^1S), is very attractive for several reasons. The energy of Ar^* is sufficient not only to ionize Ca but also to excite Ca^+ to several low-lying electronic states. The energy levels[1] of Ar^* (^3P) are compared to the relevant Ca^+ levels (referenced to a zero of energy for the neutral Ca) in Table I. From this Table, one finds that the exothermic Penning ionization channels lead to Ca^+ ($4s\ ^2S_{1/2}$), the ground state of the ion, as well as to the excited states ($4p\ ^2P^o_{1/2,3/2}$) and ($3d\ ^2D_{3/2,5/2}$). A kinetic analysis of the atomic emissions from and among these levels will lead to chemi-ionization branching ratios.

A more interesting prospect is the opportunity to observe molecular fluorescence from the excitive associative ionization products $CaAr^{+*}$. Associative ionization is known from mass spectroscopy[2] and crossed beams studies[3] to occur with appreciable probability for many chemi-ionizing collisions between two heavy reactants. However, due to the severe dynamical constraint of associative ionization -- two heavy particles collide, but

a heavy particle and a light electron result -- crossed beams methods cannot discern the internal energy distribution of associative ionization products. These products appear at the center of mass velocity as if a totally inelastic bimolecular association had occurred. To probe AI dynamics, one can measure the energy spectrum of the ejected electron[4]. This approach lacks the sensitivity and resolution of optical spectroscopy and must be carried out in a crossed beams environment with necessarily low signal intensity.

A further reason for interest in this system is the opportunity to treat the reaction as simply the source of a new molecular ion spectrum. The states of $CaAr^+$ were unknown prior to this study, but the analogous spectra[5] of $BeAr^+$, $BeKr^+$ and $BeXe^+$ have been analyzed. Due to the relatively large rotational constant of $BeAr^+$, extensive high resolution spectra were obtained by Coxon, et al.[5] A detailed analysis of the ground electronic state ($X^2\Sigma^+$) and an accurate model for the excited $A^2\Pi$ states have been published by Hartman, Goble, and Winn.[6] There is clearly little more than the pure ion-induced dipole attractive force which can be expected to bind this family of diatomics, and data on these potential curves allows this hypothesis to be rigorously examined.

These systems -- metastable rare gas + alkaline earth atoms -- also provide an interesting arena in which laser assisted processes can be studied[7]. One can access still higher states of the ionized products by coupling an intense laser field to the bimolecular collision. The frequency of this laser is not

(necessarily) tuned directly to a resonance of any isolated reagent or product, but rather to any energy difference between one reagent (the metastable) and one product (the excited aomic ion). In fact, since the entrance channel lies in a series of autoionization continua, the laser field can quite generally access normally endothermic channels of the ions products merely be raising the total energy (field + reactants) above the endothermic limit for such a channel. We have observed these effects in the Ar* + Ca system and will report our results in a subsequent article[8].

Experimental

These experiments were carried out in a flowing afterglow apparatus similar to one described previously[9]. Metastable argon, primarily $^3P_2$, was generated by a dc discharge through pure Ar at pressures near 1 torr. The flow rate ($\sim$ 1 mmole/sec) was maintained by a 1000 l/min mechanical pump. Atomic absorption measurements of the Ar* density at the reaction zone yielded values of $\sim 10^9 - 10^{10}$ atoms/cm^3. The reaction zone itself was some 35 cm downstream from the discharge. These measurements were made over the pressure range 0.4 to 1.2 torr and correspond to Ar* ($^3P_2$) absorption at 811.5 nm. The higher metastable state, $^3P_0$, is generally unobserved in the reaction zone of this apparatus. This state can be collisionally quenched to the radiating $^3P_1$ state, and it can absorb resonant discharge radiation, decaying radiatively to the ground state via several intermediate states[2b]. Since our discharge tube feeds a reaction zone of considerably greater diameter and smaller length than the discharge tube itself, the pressure in the discharge is somewhat greater than the $\sim$ 1 torr pressure of the reaction zone. This feature of the apparatus indicates that a collisional relaxation mechanism accounts for our low $^3P_0$ density. Based on the sensitivity and signal to noise characteristics of our absorption measurements, we estimate the $^3P_0$ density to be no greater than 5% of the $^3P_2$ density.

Calcium metal was held in a stainless steel oven which was radiatively heated to temperatures as high as 1000°C by

tantalum sheet heating elements. Two Ta sheets (0.010" thick) were concentrically clamped to stainless steel rings so that a large ac current could flow through one sheet and then the other, resistively heating both. The oven was suspended inside the inner sheet. Typically 400 amps of current produced a stable and uniform oven temperature. It is vital to note that the voltage drop across this heater is no more than 1 volt. As a consequence, there was no danger of producing excited Ca atoms from electron bombardment by thermionic electrons. All attempts at using high voltage, low current heaters suffered from this effect and frequently produced violent Ca discharges at the oven opening.

Ca atoms were carried to the Ar* flow by a second flow of pure Ar. This second flow swept around the oven and entrained the Ca the necessary 10 cm distance from the oven opening to the reaction zone. During this flow distance, the Ca atoms were cooled an unknown amount, but various estimates of the translational temperature for Ca in the reaction zone were always < 350K.

The reaction produces a chemiluminescent flame which is quite intense. Spectra of this flame in the wavelength region from 2000 to 8200 Å were taken with a 1.5m high-resolution scanning monochromator (Jobin-Yvon THR 1500). (Some spectra in the 8500 Å region were taken with a 0.25 m monochromator.) Depending on the type of measurement and the flame intensity, resolutions from 0.01 Å to 2 Å were used. Light was measured with a dry-ice cooled photomultiplier (RCA C31034) operated

in the pulse counting mode (dark count < 1/sec). Data collection and monochromator scanning were under computer control. A small microprocessor based computer (Commodore PET 2001) acted as a multichannel analyzer and controller, scanning a selected spectral region over and over a preselected number of times. Data were displayed on graphics plotters and stored on tape for further reduction.

The relative spectral response of the entire optical train was measured from 3200 to 8200 Å by a standard tungsten incandescent lamp of known brightness temperature.

Absolute rate constants were obtained by measuring the atomic absorption of the Ca ($^1P^0 \leftarrow {}^1S$) resonance line at 4226.73 Å. A standard hollow cathode Ca lamp was used as the light source. The line width of this Ca line was carefully measured with the 1.5 m monochromator and an absorption coefficient at the line center was calculated for a Doppler profile absorption by Ca in the flow. Due to the large oscillator strength of this transition, Ca densities could be readily measured over the range < 10^8 cm^{-3} (less than the metastable density) to > 10^{10} cm^3. The major uncertainty in this measurement was the absorption path length leading to an uncertainty in the Ca density of 20%. Given the Ca concentrations, rate constants were determined with reference to the known rate constants[10] for the Ar* + Kr → Kr* ($5p[\frac{3}{2}]_{2,1}$) + Ar reactions. Details of this method are found elsewhere.[10,11]

Results

The four strongest atomic emission features found in the flame spectra were the excitive Penning ionization lines from the reaction

$$Ar^* (^3P_2) + Ca(^1S_0) \rightarrow Ar(^1S_0) + Ca^{+*}(^2P^o_{3/2,1/2}) + e^-$$

monitored by the fast radiative cascades at 3933.66 Å and 3968.47 Å

$$Ca^{+*}(^2P^o_{3/2,1/2}) \rightarrow Ca^+(^2S_{1/2}) + h\nu,$$

and the primary atomic lines of neutral Ca, viz. the resonance line at 4226.73 Å

$$Ca(^1P^o_1) \rightarrow Ca(^1S_0) + h\nu$$

and the intercombination line at 6572.78 Å

$$Ca(^3P^o_1) \rightarrow Ca(^1S_0) + h\nu.$$

Numerous other lines of neutral Ca were observed and assigned. These lines are produced by Penning electron excitation of Ca, by electron recombination with Ca^+, and by dissociative recombination with $CaAr^+$. They were of use to us only insofar as they provided frequent wavelength markers.

The Ca^{+*} ($^2P^o \rightarrow {}^2D$) transitions near 8500 Å were observed, but are not of primary concern. Emission from the $^2P^o$ levels follows a branching ratio[12] of 6%:94% for radiating to the ^2D and ^2S states, respectively, and the total emission from $^2P^o$

levels was calculated from the $^2P^o \rightarrow {}^2S$ lines taking this into account.

Presumably, as Table I indicated, ^2D and, of course, ^2S (ground state) Ca^+ are produced. Since the ^2D levels are optically metastable, we have no data relating to their primary production rates. We also have no data relating to the ^2S primary production rate and will therefore concentrate on the $^2P^o_{3/2}$ and $^2P^o_{1/2}$ levels alone.

We observed an intensity ratio for these lines of (J = 3/2): (J = 1/2) = 5:1 at all Ca and Ar* concentrations. Since both levels have equal spontaneous emission rates[12] of 1.5×10^8 sec^{-1}, the J = 3/2 level is formed at five times the rate of the lower J = 1/2 level. Measurement of the bimolecular rate constants for production of these levels gave $k_{3/2} = 1.6 \pm 0.3 \times 10^{-10}$ cm^3-$molecule^{-1}sec^{-1}$ and $k_{1/2} = 3.2 \pm 0.6 \times 10^{-11}$ $cm^3 molecule^{-1} sec^{-1}$. These values imply thermal cross sections of 28 $Å^2$ and 5.7 $Å^2$, respectively.

To the red of these Ca^+ lines, a molecular band system was found. This system could not be associated with any known molecular spectrum. Its integrated intensity scaled with the intensity of the Ca^+ lines. We have therefore attributed this spectrum to $CaAr^+$ ($A^2\Pi \rightarrow X^2\Sigma^+$). In the shorter wavelength region of this spectrum, there are a series of overlapped and closely spaced vibrational bands. Farther to the red, a series of undulatory continua are found. A portion of this spectrum showing the bands and the first three of five continua is shown in Fig. 1. The maximum intensity of these bands was $\sim$ 200

counts/sec at 2 Å resolution, and extensive signal averaging was required to obtain a statistically reliable spectrum.

When the area under the $CaAr^+$ band was compared to the area under the Ca^+ doublet, a branching ratio of excitive associative ionization (AI*) to excitive Penning ionization (PI*) was found to be AI*:PI* = 14%:86%, implying an AI* rate constant of $3.1 \pm 0.6 \times 10^{-11}$ $cm^3 molecule^{-1} sec^{-1}$, or a cross-section of 5.5 $Å^2$.

Discussion

Before turning to a detailed discussion of the kinetic results and a discussion of our spectral analysis of the $CaAr^+$ bands, some general comments are in order. Penning ionization has been given a lucid theoretical interpretation by Miller and co-workers.[13] At its simplest, PI involves a two electron energy exchange: the readily ionized electron on the target Ca fills the 3p vacancy in Ar* while the excited 4s electron of Ar* leaves the scene, becoming the ionized electron.

To explain the production of excited states of the ion, one must elaborate this model to include collision configuration mixing, much in the way one treats photoelectron ejection[14] to excited ionic states. In terms of what Shirley[14] has called initial state configuration interaction, one recognizes that $ns^2\ ^1S$ ground states can also mix np^2, nd^2, etc. ^1S coupled configurations. Thus, np, nd, etc. ion states are observed as photoemission satellites. For collisional ionization, it is more appropriate to follow the molecular orbital correlation diagram shown in Fig. 2. On the right, energies of the atomic orbitals of the reactants are ordered with respect to a zero of energy for $Ca^+ + Ar + e^-$. Similar energies for the separated product orbitals are shown on the left. These orbitals are correlated to the united atom limit (Sr) toward the center of the figure. The box in this column labeled 5p-4d represents the range of energies assumed by these orbitals for Sr and Sr^+. Electron populations are shown for a collision resulting in ground state

Ca^+, but, as indicated by the correlations, the 4p Ca^+ orbital is derived from the same set of UA levels. The change in energy of these levels with ionization and with atomic separation is an indication of the correlation effects which couple the reactants to the various product states.

These arguments do not directly relate to the final populations of the fine structure components of any given product term. Schearer and co-workers[15] have performed beam experiments with He^+ and various alkaline earths which have demonstrated collisional alignment of $^2P^o_{3/2}$ ion levels. In particular, coherent excitation was observed[15a] from Sr^+ ($5p\ ^2P^o_{3/2}$) *via* the linear polarization of the fluorescence. These authors sketch a theory for this alignment which specifically neglects electron spin; spin is neglected because their experiments yielded a statistical population of the $5p\ ^2P^o$ fine structure states of Sr^+. Similarly, Ebding and Niehaus[16] found statistical populations in the Penning electron peak heights from He* ionizations of Ar, Kr, Xe, and Hg to the $^2P^o_{1/2,3/2}$ states of the rare gas ions and the $^2D^o_{5/2,3/2}$ state of Hg^+. These results are at variance with our observation that $Ca^+(4p\ ^2P^o_{3/2})$ is populated at a rate five times that of the Ca^+ ($4p\ ^2P^o_{1/2}$) state.

A simple propensity to conserve total electronic angular momentum would favor $^2P^o_{3/2}$ production in our experiments. To conserve orbital electronic angular momentum, the ejected electron must be an s-wave. The total electronic angular momentum is carried by $Ar^*(^3P_2)$. The total product angular momentum of the pair $e^-(^2\ _{1/2}) + Ca^+(^2P^o_{3/2})$ conserves this quantity.

To generate the term symbols for the autoionizing surfaces of Ar* + Ca, one must begin, at large separations, following Hund's case (c) coupling. These surfaces can be correlated to case (a) or (b) terms at smaller distances, In case (c), $^3P_2$ + $^1S_0$ combine to form 2, 1, and 0^- states. These states become $^3\Pi_2$ and $^3\Sigma^+$ in case (a) and (b), respectively. The $^3P_2$ state of Ar* (more accurately denoted the $[3/2]_2^o$ state since LS coupling is inappropriate for these states of Ar) is the only excited state of Ar with appreciable population in our experiments. (The $^3P_1$ level correlates to $^3\Pi_1$ and $^3\Pi_{0^+}$; $^3P_0$ correlates to $^3\Pi_{0^-}$.) With He* ($2\ ^3S_1$) + any $^1S_0$ atom, only the 1, 0^- (or $^3\Sigma^+$) states arise. Riseberg, et al.,[17] have used the propensity rule for conservation of electronic orbital angular momentum to explain why Π molecular states lead to less ground state ion product ($^2S_{1/2}$ Cd^+ and Zn^+ in their experiments) than Σ states. Thus, the non-statistical population of Ca^+ $^2P^o$ fine structure levels in our experiment is due to the propensity to conserve total electronic angular momentum, the presence of the $^3\Pi_2$ autoionizing state, and the non-statistical population of the ^3P levels of our Ar* reagent.

While we do not measure the total ionization cross-section (or, almost equivalently, the total metastable quenching cross-section), we have estimated this quantity from an orbiting model. Here we assume any collision with an impact parameter leads to ion production. We assume a single attractive reactant surface of the form $V_0 = -C_6/R^6$ with C_6 approximated by the London formula. This model yields a total ionization thermal rate

constant of 6×10^{-9} $cm^{-3} molecule^{-1} sec^{-1}$. This is only a crude model which is likely to overestimate the total ionization rate. Therefore, we expect the true fraction of reactive collisions which lead to fluorescence to be at least the 4% predicted by this model and probably somewhat more.

We turn now to the $CaAr^+$ bands. The $CaAr^+$ $A^2\Pi \rightarrow X^2\Sigma^+$ system should derive its oscillator strength from the corresponding Ca^+ atomic transitions. The lifetimes of the $^2P^o$ states of Ca^+ are 6.7 nsec.[12] Thus, even at a pressure near 1 torr, the $CaAr^+$ emission should be representative of the nascent $CaAr^+$ ($A^2\Pi$) distribution. (The ion-molecule collision rate at 1 torr is ca. 10^8 sec^{-1}.)

Due to the weakness, spectral extent, and spectral congestion of the $CaAr^+$ emission, we were unable to resolve rotational features. It is likely that the molecule is highly excited rotationally due to the inability of the Penning electron to remove the initial collisional angular momentum. Visual inspection of the spectrum suggests a high vibrational excitation as well. The emission is found to contain bound-bound transitions of many closely spaced vibrational progressions as well as continuum bound-free features extending well to the red.

To analyze this spectrum, we have used model potential functions for the upper and lower states. The analysis of $BeAr^+$ by Goble, et al.[6], demonstrated that these molecular ions are well represented by a model potential of the form

$$V(R) = A \exp(-BR) - Z^2 e^2 \alpha / 2R^4$$

where α is the polarizability[18] of Ar (1.64 $Å^3$) and A, B, and Z are parameters. This (exp - Z4) potential incorporates the physical picture of ion-induced dipole attraction, but by an ion of (perhaps) non-integral charge, to account for the effects of incomplete nuclear shielding by the outer electrons of Ca^+ in the vicinity of the equilibrium position. For the ground state ($X^2\Sigma^+$) of $CaAr^+$, one expects $Z \sim 1$ due to the $4s\sigma$ orbital on Ca^+. For the $A^2\Pi$ state, one expects $Z \sim 2$, since this state corresponds to the $4p\pi$ Ca^+ excitation. The $p\pi$ electron is considerably less effective in screening the nuclear charge. A related consequence of this excitation is the prediction that $R_e(A) < R_e(X)$. This bond length trend is observed in $BeAr^+$ and will be seen to be of importance in explaining $CaAr^+$ emission.

We have used these model potentials to synthesize the $CaAr^+$ spectrum with the following assumptions. First, in accord with the preponderance of atomic excitation into $^2P^o_{3/2}$ over $^2P^o_{1/2}$, we have assumed only a single excited state (i.e., $A^2\Pi_{3/2}$). The $^2\Pi_{1/2}$ emission is assumed to be weak and unimportant. Consequently the asymptotic limit of the two potentials (A and X) was set at the $^2P^o_{3/2} \rightarrow {}^2S_{1/2}$ Ca^+ transition energy of 25414 cm^{-1}. We note that the atomic combination $^2P^o_{3/2} + {}^1S_0$ can also lead to the molecular $B^2\Sigma^+$ state. We have no evidence of fluorescence from this state, and neglected it in our analysis.

Our second assumption involved the parameters of the model potentials. We have set the effective nuclear charge parameters,

Z, at 1.0 and 2.0 for the ground and excited states, respectively. Our data were not sufficiently sensitive to allow us to fit all three parameters of each state. We chose to fix Z, since this is the parameter with the most obvious physical interpretation. For $BeAr^+$, the corresponding Z values were found[6] to be $Z_\Sigma = 1.29$ and $Z_\Pi = 1.88$. One expects Z_Σ to decrease with increasing ion size and Z_Π to increase.

To simulate the spectrum, the remaining parameters of the potentials (which were input as R_e and ω_e values) were used in the following scheme and systematically varied to improve the fit. Vibrational energy levels were calculated by either a semi-classical (Bohr-Sommerfeld) method or by direct numerical integration of the radial Schrödinger equation. Franck-Condon factors were calculated using numerical bound and continuum wavefunctions from a direct integration. From these data, spectral frequencies and bound-free continuum oscillations were synthesized.

The blue limit of the continuum emission from a particular $A^2\Pi$ vibrational level is particularly informative in this type of fitting procedure. The difference between this limit and the asymptotic ($^2P^o_{3/2} \rightarrow {}^2S_{1/2}$) limit gives the energy of the vibrational level measured from the dissociation limit of $A^2\Pi$. From our data, this energy is around 1000 cm^{-1}. The continuum limit also serves another purpose. The band spacing to the blue of this limit (in the bound-bound portion) is around 50 cm^{-1}, and a quick check of this portion of the synthesized spectra allowed us to reject poor potential constants.

The best fit was obtained with the parameters Z = 1, ω_e = 87 cm^{-1}, and R_e = 2.8 Å for the $X^2\Sigma^+$ state and Z = 2, ω_e = 200 cm^{-1}, and R_e = 2.6 Å for the $A^2\Pi$ state. The dissociation energies are 1000 cm^{-1} (X) and 4900 cm^{-1} (A) with estimated uncertainties of ± 100 cm^{-1} in each. These potentials are shown in Fig. 3, and a comparison between the observed and simulated spectra is given in Table II.

Our observation that $CaAr^+$ $A^2\Pi$ is formed in vibrational levels within 1000 cm^{-1} of dissociation is consistent with Penning electron results[4]. These measurements, on He* + Kr, Xe, Na, K, and Hg, find AI products formed with energies from ∿ 800 to 6000 cm^{-1} below the dissociation limit. While the CaAr* autoionizing states are not directly exposed by these experiments, they are expected to be less strongly bound than $CaAr^+$ ($X^2\Sigma^+$), since they lack ion-induced dipole attractions. They should also have longer bond lengths than the molecular ion states, due to the earlier onset of repulsion from the combination of larger atoms (Ar* and Ca). Thus, with an autoionization rate increasing with decreasing distance, a localized, vertical AI at or near the radial turning point of the CaAr* collision would produce $CaAr^+$ at the outer turning point of a high vibrational level, as observed.

Conclusions

The Ar* + Ca chemi-ionization reactions have certain characteristics reminiscent of other types of electronic energy transfer reactions. Due to the dynamic constraint of the small product reduced mass, associative ionization has much in common with associative detachment and radiative association. The experiments reported here demonstrate that metastable + alkaline earth collisions, with a wide variety of product states, symmetries, and exothermicities available, are a valuable source of information on the dynamics of these processes.

With Ar* + Ca, we have observed the partial transfer of fine structure polarization in Ar* to the Ca^+ ^2P levels, the emission spectrum of the associated ion, and the nascent internal energy distribution of this ion. Further experiments of this type or of the type recently reported[20] in a direct discharge of Xe and Mg should continue to provide such information.

Acknowledgement

This work was supported in part by the National Science Foundation and in part by the Research Corporation, and the U.S. Department of Energy under Contract W-7405-ENG-48.

Figure Captions

Fig. 1. Spectrum of $CaAr^+$ from 3980 to 4220 Å at 1 Å at 1 Å resolution. The three sharp features near the center of the spectrum are weak atomic Ca lines. The rising intensity at the right of this figure is the blue wing of the strong 4227 Å Ca resonance line overlapped with a $CaAr^+$ continuum oscillation.

Fig. 2. Molecular orbital correlation diagram connecting the separated atoms of the reacants, Ca + Ar*, and the product, Ca^+ + Ar, to the united atom limit, Sr. The UA orbitals which change energy significantly on going from Sr to Sr^+ are outlined in the shaded box, indicating the source of configuration mixing leading to excited ion products.

Fig. 3. (EXP-Z4) model potentials for $CaAr^+$ which give the best fit to the observed spectrum. Shown schematically are the inner turning point bound-free transitions and the outer turning point bound-bound transitions for v' = 28 to 31.

Table I. Energy levels of Ar* and Ca^+ referenced to an Ar + Ca zero of energy, from Ref. 1.

Species	Energy (cm^{-1})
Ar* ($^3P^o_2$ $[\frac{3}{2}]^o_2$)	93,144
Ca^+ (4p $^2P^o_{3/2}$)	74,720
Ca^+ (4p $^2P^o_{1/2}$)	74,498
Ca^+ (3d $^2D_{5/2}$)	63,017
Ca^+ (3d $^2D_{3/2}$)	62,956
Ca^+ (4s $^2S_{1/2}$)	49,306

Table II. Observed and calculated frequencies for $CaAr^+$, in vacuum wavenumbers.

Observed	Calculated[c]				Type of Transition
	v'=28	v'=29	v'=30	v'=31	
22562	22560	22625	22680	22720	Bound-free
23792	23750	23820	23880	23950	Bound-free
24044 24266	24130	24100	24160	24230	Bound-free[a]
24543	24546	-----	-----	-----	Bound-bound[b]
24598	-----	24600	-----	-----	Bound-bound
24650	-----	-----	24652	-----	Bound-bound
24695	-----	-----	-----	24701	Bound-bound

(a) These overlapped transitions together combine to form the two observed oscillations.

(b) Transition frequencies with the largest Franck-Condon factor.

(c) These quantum numbers are model potential dependent and may be in error by, at most, $\Delta v' = 2$.

References

1. C.E. Moore, Natl. Stand. Ref. Data Serv. Natl. Bur. Stand. 35 (1971).

2. a) A. Fontijn, Prog. React. Kinet. 6, 75 (1971); b) further details of metastable rare gas production, detection and chemistry may be found in D.H. Stedman and D.W. Setser, Prog. React. Kinet. 6, 193 (1971).

3. H. Haberland, Y.T. Lee, and P.E. Siska, in "The Excited State in Chemical Physics, Part 2", J.Wm. McGowan, ed. (Wiley-Interscience, N.Y., 1979).

4. H. Hotop and A. Niehaus, Z. Physik 315, 395 (1968); ibid. 228, 68 (1969); ibid. 238, 452 (1970); V. Fuchs and A. Niehaus, Phys. Rev. Lett. 21, 1136 (1968); V. Cermak, Coll. Czech. Chem. Comm. 33, 2739 (1968); V. Cermak and Z. Herman, Chem. Phys. Lett. 2, 359 (1968).

5. K.V. Subbaram, J.A. Coxon and W.E. Jones, Can. J. Phys. 54, 1535 (1976); J.A. Coxon, W.E. Jones, and K.V. Subbaram, Can. J. Phys. 55, 254 (1977); ibid. 53, 2321 (1975).

6. J.H. Goble, D.C. Hartman, and J.S. Winn, J. Chem. Phys. 67, 4206 (1977).

7. J.S. Winn, in Advances in Laser Chemistry, A.M. Zewail, ed., Springer Series in Chemical Physics, Springer, Berlin, (1978), p. 426.

8. J.H. Goble and J.S. Winn (unpublished results).

9. D.C. Hartman, W.E. Hollingsworth, and J.S. Winn, J. Chem. Phys. 72, 833 (1980).

10. L.A. Gundel, D.W. Setser, M.A.A. Clyne, J.A. Coxon, and W. Nip, J. Chem. Phys. 64, 4390 (1976); corrections to this paper, pointed out in L.G. Piper, J. Chem. Phys. 67, 1795 (1977), were applied.

11. D.C. Hartman, Lawrence Berkeley Laboratory Report LBL 9819, (1979) (Ph.D. Thesis).

12. W.L. Wiese, M.W. Smith, and B.M. Miles, Natl. Bur. Stand. U.S. Circ. 22 (1969).

13. W.H. Miller, J. Chem. Phys. 52, 3563 (1970).

14. D.A. Shirley, J. de Phys. 39, C4-35 (1978). See also S. Suzer, S.T. Lee, and D.A. Shirley, Phys. Rev. A 13, 1842 (1976).

15. (a) D.W. Fahey, L.D. Schearer, and W.F. Parks, Phys. Rev. A 20, 1372 (1979); (b) L.D. Schearer and L.A. Riseberg, Phys. Rev. Lett. 26, 599 (1971); (c) W.F. Parks and L.D. Schearer, Phys. Rev. Lett. 29, 351 (1972); (d) D.W. Fahey, W.F. Parks and L.D. Schearer, J. Phys. B 12, L619 (1979).

16. T. Ebding and A. Niehaus, Z. Phys. 270, 43 (1974).

17. L.A. Riseberg, W.F. Parks and L.D. Schearer, Phys. Rev. A 8, 1962 (1973).

18. A. Dalgarno and A.E. Kingston, Proc. Roy. Soc. (London) A259 424 (1961).

19. J.W. Cooley, Math. Computation 15, 363 (1961); J.K. Cashion, J. Chem. Phys. 39, 1872 (1963).

20. L. Schumann, D. Wildman, and A. Gallagher, J. Chem. Phys. 72, 6081 (1980).

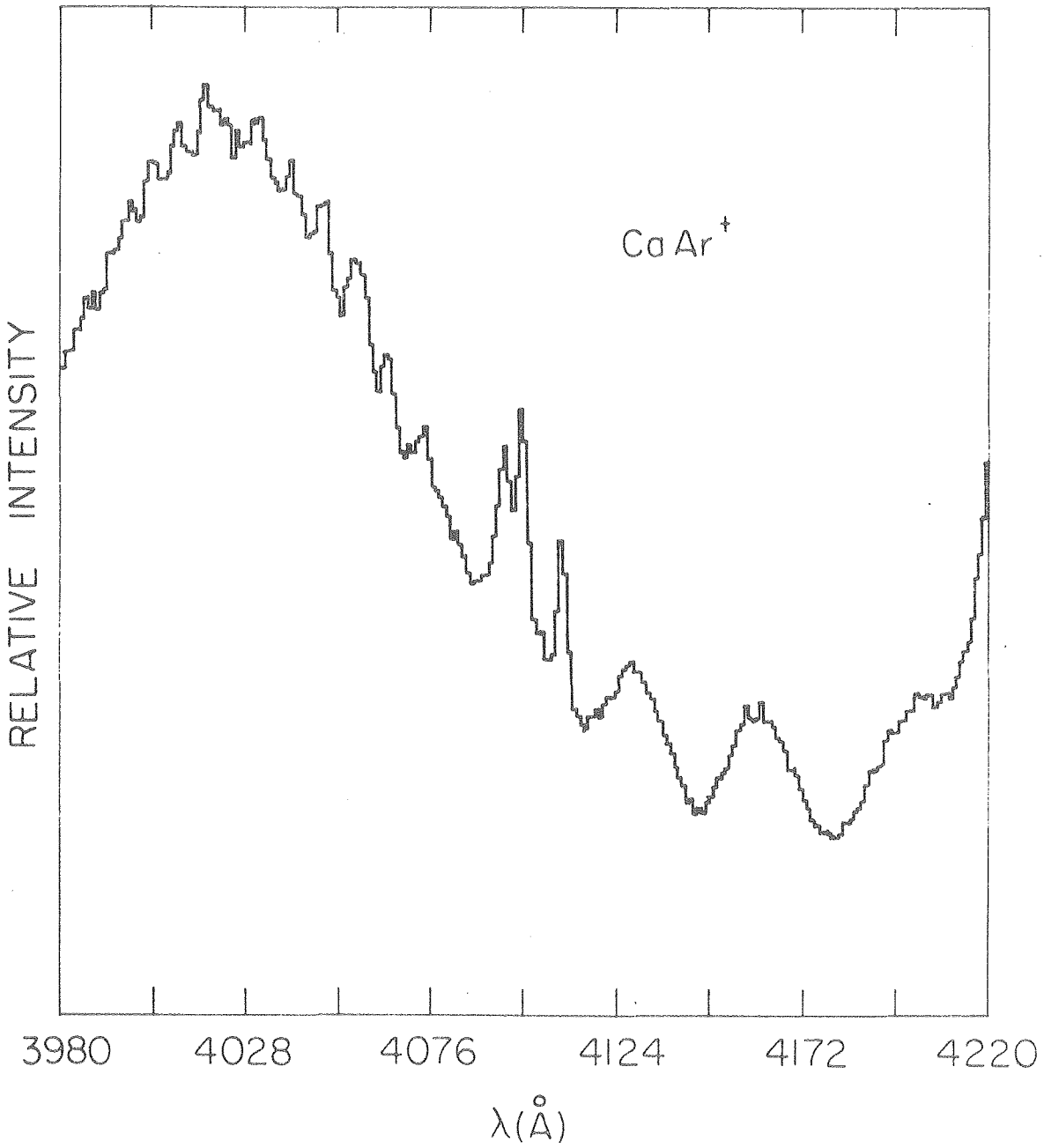

XBL-7910-12400

Figure 1

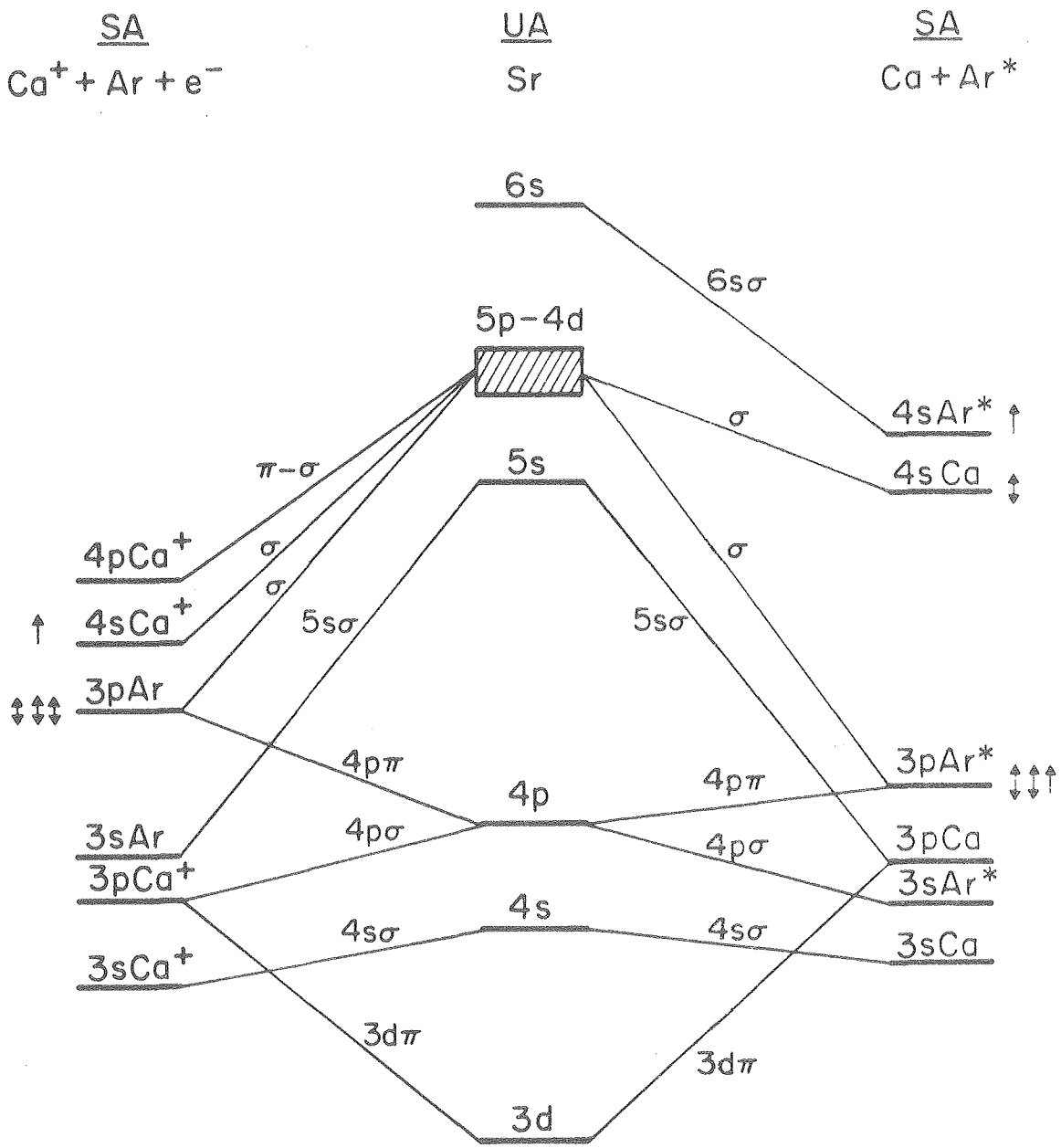

XBL-8012-12915

Figure 2

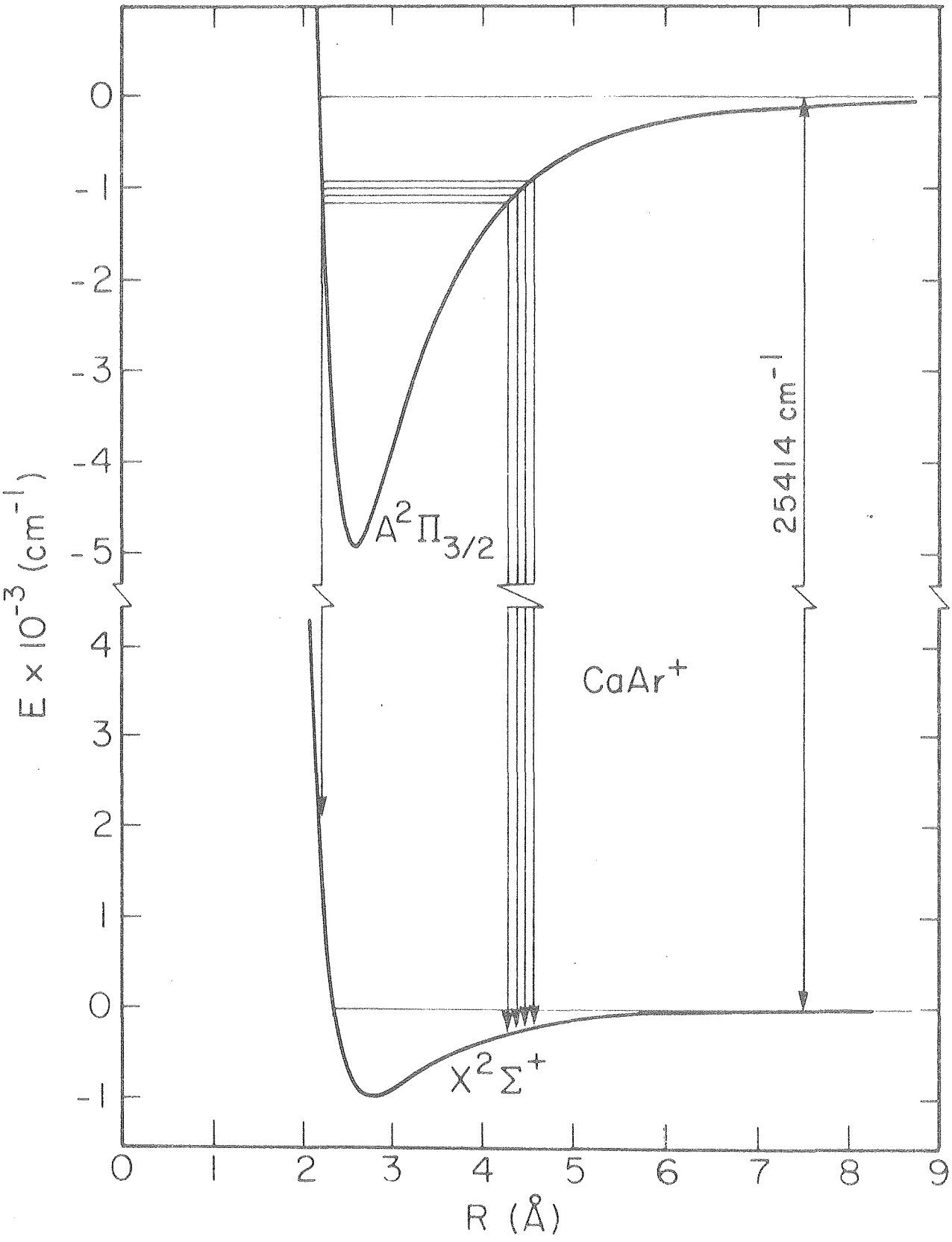

XBL-7910-12397

Figure 3